Space Sci Rev (2007) 132: 575–591
DOI 10.1007/s11214-007-9282-3

Plasma Waves in the Hermean Magnetosphere

L.G. Blomberg · J.A. Cumnock · K.-H. Glassmeier · R.A. Treumann

Received: 2 July 2007 / Accepted: 24 September 2007 / Published online: 9 November 2007

Abstract The Hermean magnetosphere is likely to contain a number of wave phenomena. We briefly review what little is known so far about fields and waves around Mercury. We further discuss a number of possible phenomena, including ULF pulsations, acceleration-related radiation, bow shock waves, bremsstrahlung (or braking radiation), and synchrotron radiation. Finally, some predictions are made as to the likelihood that some of these types of wave emission exist.

Keywords Mercury · Magnetosphere · Plasma waves · Pulsations · Magnetospheric radiation

1 Introduction

Mariner 10 found, somewhat surprisingly, that Mercury possesses a sufficiently strong internal magnetic field for a proper magnetosphere to be set up as the solar wind flows by. The dipole moment of Mercury has been estimated in the range 200–400 nT R_H^3 where R_H is the Hermean radius, 2,440 km. The uncertainty in the estimate stems from the fact that the only available in situ magnetic data from Mercury were collected during Mariner 10's two near flybys, which is not sufficient to fully constrain the field. In addition, because of the relatively weak planetary field and the comparatively strong interplanetary magnetic field,

L.G. Blomberg (✉) · J.A. Cumnock
Space and Plasma Physics, School of Electrical Engineering, Royal Institute of Technology, Stockholm, Sweden
e-mail: lars.blomberg@ee.kth.se

K.-H. Glassmeier
Institute of Geophysics and Extraterrestrial Physics, Technical University of Braunschweig, Braunschweig, Germany

R.A. Treumann
Geophysics Section, Department of Geophysics and Environmental Physics, The University of Munich, Munich, Germany

Table 1 Typical solar wind parameters at Mercury

Velocity	300–800 km/s
Density	30–70 cm^{-3}
Magnetic field	20–40 nT
Ion temperature	11–16 eV
Electron temperature	17–21 eV

even with a larger data set the problem of separating the planetary and the interplanetary fields will remain.

Balance between the solar wind dynamic pressure and the planetary magnetic field typically results in a magnetopause stand off distance in the range 1.2–1.5 R_H, although it is believed that under extreme solar wind conditions the solar wind may impact directly on the dayside surface of the planet. Typical values of the solar wind parameters at the position of Mercury are given in Table 1.

The interaction of the solar wind with the planetary magnetic field also sets up a potential drop across the magnetosphere, typically in the range 5–25 kV, corresponding to a cross-tail electric field of 1–5 mV/m. These numbers assume an interaction similar to that at Earth, which is probably a valid assumption under normal solar wind conditions. However, under more extreme solar wind conditions, the cross-polar potential at Earth is known to saturate, an effect that has been attributed to the existence of a field-aligned current system on the dayside. The associated closure currents produce a magnetic field at the magnetopause which counteracts the magnetospheric field and, thus, weakens reconnection. However, because of the low conductivity of the Hermean (exo)ionosphere it is unclear whether a similar current system is set up at Mercury, which in turn means that a saturation effect similar to that at Earth may or may not exist at Mercury (Blomberg et al. 2006).

The interaction of the solar wind with the magnetosphere may also result in wave activity at a variety of frequencies. Figure 1 shows an overview of the wide variety of wave emissions that are expected at Mercury. In this paper, we discuss a selection of these different phenomena in more detail. The first comprehensive investigation of the wave spectrum around Mercury will be performed by the PWI instrument (Matsumoto et al. 2006) onboard the BepiColombo spacecraft. Until BepiColombo arrives at Mercury most of the topics discussed in this paper will remain speculative.

At the lower end of the spectrum we find ULF waves, which have been observed at Mercury (Russell 1989). Although ULF waves at Mercury may be conceptually similar to those at Earth, their physics are different. At Earth ULF waves have frequencies well below all relevant gyro frequencies in the system. However, at Mercury, the wave frequency is typically comparable to or even greater than the gyro frequencies of one or more particle species. This makes an MHD description irrelevant and leads to wave characteristics that depend on the plasma composition in an interesting way. Another interesting difference is found in the potential driver mechanisms for ULF waves, which we will return to later.

At the higher end of the spectrum we find radiation in the radio and X-ray bands. This is of particular interest at Mercury since its potential observation offers the possibility of remotely inferring the conditions in the radiation source regions. So far, however, observations of radiation have been unsuccessful. The reason for this might be that radiation has not been given enough attention; or that radiation is completely absent. We investigate the conditions under which radio radiation and natural X-rays can be expected to be emitted from Mercury. In principle, we can distinguish four types of radiation expected to be emitted from a strongly magnetized planet, some of them we would also expect to occur at Mercury. The first type is radiation in the radio band generated at the planetary bow shock or—more

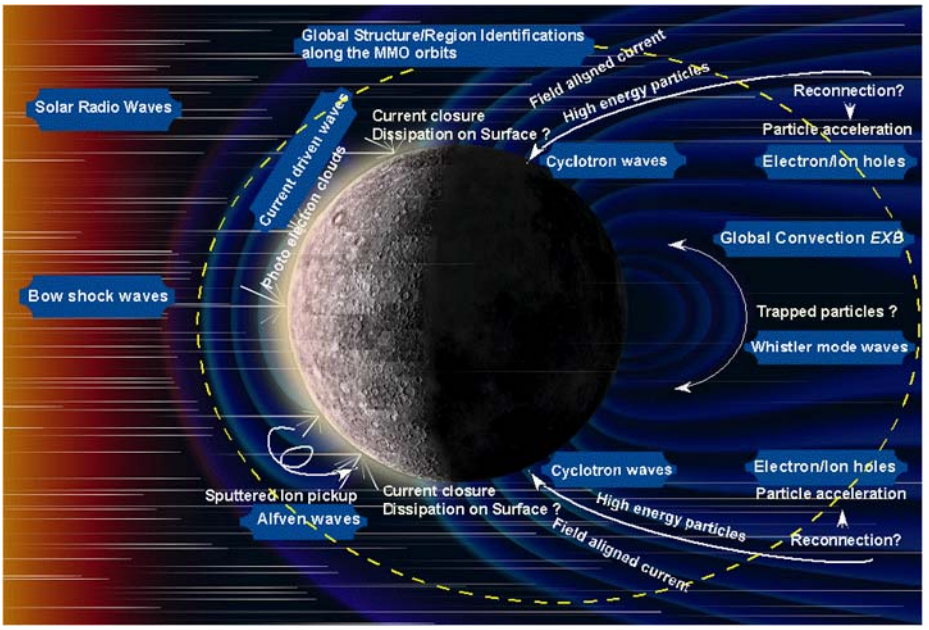

Fig. 1 Overview of expected wave activity in the Hermean magnetosphere. After Matsumoto et al. (2006)

precisely—in the electron foreshock of the planetary bow shock. The second type is the emission of synchrotron radiation. The third type is radio radiation from Mercury's auroral magnetosphere. Finally, the fourth type is X-ray emissions from the potential auroral regions on Mercury. A question of particular interest here is: Is there any equivalent at Mercury to the auroral kilometric radiation of Earth and the hectometric radiation from Jupiter? We will return to all four of these types of radiation in the following.

2 Ultra-Low Frequency Waves

Ultra-Low Frequency (ULF) waves are well known from the terrestrial magnetosphere. On the global scale we find the Pc5 type of waves, sometimes referred to as field-line resonances (Tamao 1965; Southwood 1974; Chen and Hasegawa 1974). These waves are standing oscillations on the magnetic field lines that bounce back and forth between the northern and southern ionosphere. In simple terms these waves arise when a fast mode wave is somehow generated and subsequently propagates across the magnetic field until it reaches a turning point where the fast mode and the shear Alfvén mode are in resonance, where part of the fast mode energy is coupled into the field-aligned mode and part of that energy is reflected. The fast mode wave may be generated by either a Kelvin–Helmholtz instability at the magnetospheric flanks, solar wind pressure pulses impinging on the magnetopause, or wave-particle interaction processes within the magnetosphere.

At Earth the ionosphere is a reasonably good conductor (compared to the effective conductance of the flux-tube waveguide) and therefore acts to more or less "short circuit" the wave electric field at the reflection points, resulting in a significant fraction of the wave energy being reflected back up along the field line. If the short circuiting is not perfect some

wave energy will be dissipated into the ionosphere leading to damping of the wave unless energy is continuously being fed into it somewhere else. In the (unlikely) case of matching between the waveguide and reflection surface conductances, all of the wave energy would be transmitted into the ionosphere and thus there would be no reflected wave. In case the reflection surface is a poor conductor compared to the waveguide, the wave magnetic field rather than the wave electric field would be reduced (or short circuited, in the extreme case) still resulting in a reflected wave, although differently polarized from the case of a well-conducting reflecting surface. Although the latter case is not likely to occur at Earth, it cannot be ruled out at Mercury.

In the terrestrial magnetosphere, the bounce period between hemispheres for ULF waves is on the order of minutes, which corresponds to frequencies that are lower than the ion cyclotron frequencies of the ionospheric ions by several orders of magnitude. Thus, an MHD description is relevant and the waves are found to be shear Alfvén waves. At Mercury the situation is quite different. The bounce period is of the same order of magnitude as the proton cyclotron frequency and, thus, an MHD description is not immediately applicable. Othmer et al. (1999) and Glassmeier et al. (2004, 2003) addressed this problem with a multi-ion model and found what they called a crossover frequency at which the plasma supports a completely guided mode (corresponding to the transverse MHD mode). The crossover frequency depends on the ion composition. In the case of a two-ion plasma it lies in between the two ion cyclotron frequencies.

Using the multi-ion model the ion composition in the magnetosphere may be estimated. For a plasma with two ion species a direct estimate is obtained, whereas for a plasma with more than two ion species, further information or assumptions are needed. We exemplify this using Mariner 10's observations of a ULF wave at Mercury first published by Russell (1989); see Fig. 2. The waves are mostly transverse with a period of 2 s. Russell (1989) estimated the Alfvén wave bounce time between hemispheres to be 8 s and, thus, concluded that the observed wave could be the fourth harmonic of a standing wave. Othmer et al. (1999) applied their multi-ion model to the Mariner 10 data and derived a 14% (number density) sodium content, assuming protons and sodium as the only ion species. By including helium

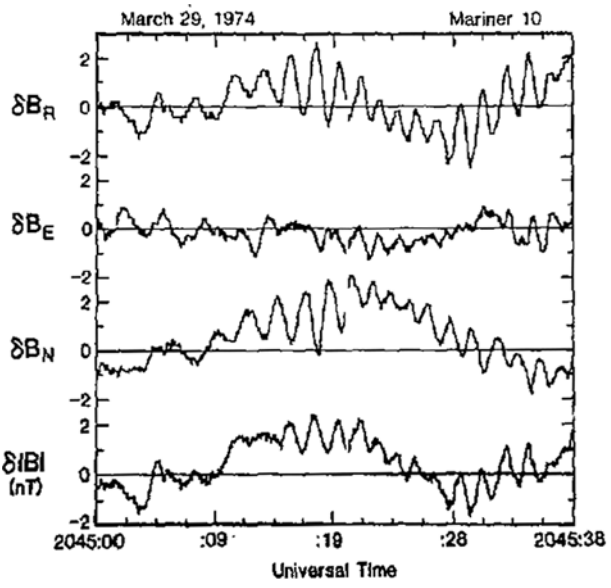

Fig. 2 ULF waves in Mercury's magnetosphere detected by the Mariner 10 magnetometer. After Russell (1989)

with a helium-to-proton ratio equal to that found in the solar wind, their model yielded an estimate of the sodium content of 20%.

ULF waves in Mercury's magnetosphere may also help understand the reflective and/or conductive properties of the planetary surface and/or low-altitude plasma, provided that both the electric and magnetic field are measured. From the phase difference between the electric and the magnetic field in a standing wave, the reflection coefficient at the boundary may be determined, which in turn gives information on the conductivity of the boundary relative to the waveguide conductivity. Thus, a properly instrumented satellite observing a ULF wave would remotely sense the conductivity of the planet at the magnetic footpoint.

Finally, a note on the driver mechanisms for ULF waves. In the terrestrial case, there are several instabilities within the magnetosphere that may drive waves via wave–particle interaction. However, some of these may be less likely to occur at Mercury since they are dependent on energetic particles bouncing and drifting in the planetary magnetic field. Mercury's small magnetosphere may not be able to contain sufficiently energetic ions in trapped orbits for the instabilities to develop.

3 Auroral Conditions at Mercury

All other magnetized planets in the solar system—Earth, Jupiter, Saturn, Uranus, and Neptune—are known to emit intense radio radiation from their auroral zones. Figure 3 shows a recent compilation of the known radio spectra of the planets. In addition, the auroral zones of the magnetized planets are subject to radiation of sporadic X-ray bursts that are related to electrons which have become accelerated in the auroral regions and precipitate into the planetary atmosphere.

The most intense planetary radiation is connected with the auroral activity of the planet, unless driven by the interaction of moons with the planet and the planetary magnetosphere. The latter is the case for the interaction of Jupiter with its satellite Io (Fig. 4).

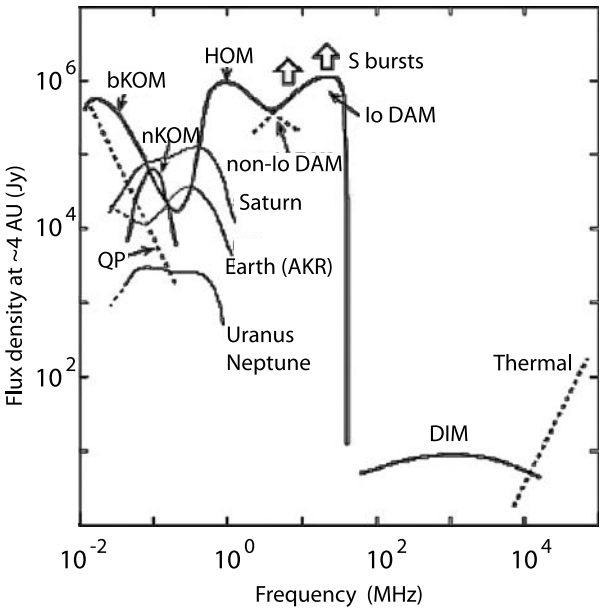

Fig. 3 Compilation of the known radio spectra emitted from the magnetized planets in the solar system (courtesy American Geophysical Union, after Zarka (1998)). The largest and most intense variety of radiation types is found for Jupiter covering the range from kilometric (KOM) through hectometric (HOM) to dekametric (DAM) wavelengths and includes Io-related radiation as well as quasiperiodic emissions (QP). Highest flux densities are found in Jupiter's S-shaped (in a frequency-time diagram) bursts. DIM in this figure indicates the decimetric solar radiation. At high frequencies the thermal galactic background radiation takes over

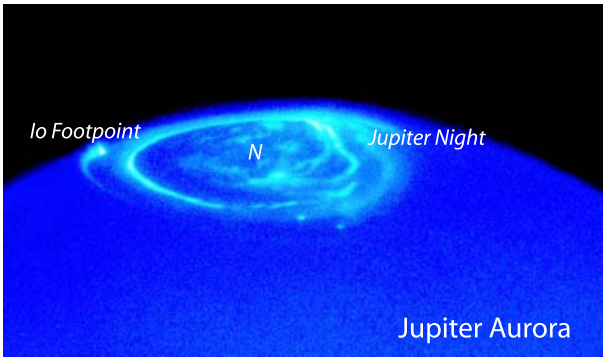

Fig. 4 Aurora on Jupiter, the largest and most strongly magnetized planet in the solar system. The aurora is seen here in a Hubble Space Telescope UV recording encircling the north pole of the planet (courtesy NASA/ESA/J. Clarke). The bright spot on the Jovian dayside is the footpoint of the magnetic flux tube that connects Jupiter's moon Io with the planet. The auroral oval maps the Jovian plasma sheet boundary region to the planetary atmosphere. Auroral substorm activity is seen from the evening through midnight to the morning sides in striking similarity to Earth, indicating substorm activity and thus reconnection in the Jovian tail plasma sheet even though the dynamics of the Jovian magnetosphere is different from that of the Earth and more resembles that of pulsars in that it is dominated by the planet rotation, indicating that substorms are a general phenomenon being insensitive to the nature of the gross magnetospheric dynamics and the cause of magnetospheric convection. For the slow rotator Mercury this implies that substorms will occur in the Hermean magnetosphere as well as long as a plasma sheet is formed in its magnetospheric tail

So far, no auroral radio emissions or auroral X-rays from Mercury have ever been reported. Therefore the intriguing question arises whether the Hermean conditions allow for generation of radiation. From in situ observations in the Earth's auroral zone and from remote observations of the Jovian radiation it has been established that the emissions are generated by the electron–cyclotron maser mechanism (for reviews see Zarka 1998; Treumann 2006) under the condition that the plasma density is very low and the electrons are at least weakly relativistic with bulk relativistic gamma factor γ_{rel}. These conditions can be written as

$$\frac{\omega_{pe}^2}{\omega_{ce}^2} \ll 1, \tag{1}$$

and

$$\gamma_{rel} - 1 > \frac{\omega_{pe}^2}{4\omega_{ce}^2}. \tag{2}$$

Hence, the electron plasma frequency ω_{pe} should be much less than the (nonrelativistic) electron cyclotron frequency ω_{ce} which implies that the Hermean magnetic field B_M must be correspondingly strong. $\gamma_{rel} - 1$ is the relativistic kinetic energy factor of the electrons that are responsible for the emission of the radiation. This condition is not very strong since by the first condition the right-hand side is small. If both conditions are satisfied, the radiation is emitted at frequency

$$\omega = \omega_{ce}(1 - \delta), \tag{3}$$

where $0 < \delta \ll 1$ so that the radiation frequency is just below but close to the electron cyclotron frequency ω_{ce}. In terms of the electron cyclotron frequency the maximum growth

rate of the maser instability becomes

$$\frac{\Gamma_m}{\omega_{ce}} \approx \frac{\omega_{pe}}{\omega_{ce}} \sqrt{\frac{k_B T_e}{m_e c^2}} = \frac{\omega_{pe}}{\omega_{ce}} \sqrt{\gamma_{rel} - 1}, \tag{4}$$

where $0 < \gamma_{rel} - 1 \ll 1$ and $k_B T_e = (\gamma_{rel} - 1) m_e c^2$ is the thermal kinetic energy of the radiating electrons. Since both factors on the right-hand side of this equation are small, the linear growth rate of the maser radiation is much less than the electron cyclotron frequency. Its lower limit is given by

$$\Gamma_m > \frac{1}{8} \left(\frac{\omega_{pe}}{\omega_{ce}} \right)^3 \omega_{ce}. \tag{5}$$

From expressions (1–5) one immediately realizes that it is not easy to satisfy the conditions for any detectable auroral maser emission from Mercury unless the density in the radiation source region becomes very small. For the measured Hermean plasma sheet electron densities are $n_e \sim 3 \times 10^6$ m^{-3} (Ogilvie et al. 1977) and near-surface magnetic field strengths are $B_M \sim 300$ nT (Ness et al. 1975; Russell et al. 1988); the frequency ratio is $\omega_{pe}/\omega_{ce} \sim 2$, which violates the first condition. In addition, higher relativistic particle energies are required in order to obtain positive growth rates. There is also the possibility that the plasma sheet density varies significantly. Mukai et al. (2004) predicted plasma sheet densities in the range 0.1–32 cm^{-3} which, if correct, would mean that the radiation condition may sometimes be satisfied. The above conditions apply to maser radio-emission near the electron cyclotron frequency. At higher harmonics of the cyclotron frequency the conditions become less severe. Positive growth rates are obtained then even for plasma-to-cyclotron frequency ratios larger than one. Under Hermean conditions this implies emission frequencies >17 kHz. Radiation will then be emitted at oblique angles with respect to the magnetic field. Although this favors escape to free space, the expected growth rates are rather small for two reasons. First, the growth rates decrease with the square of the harmonic number. Second, the oblique resonance condition ceases to be circular. It becomes a displaced ellipse in momentum (velocity) space, only a small part of which matches the positive perpendicular phase space gradient of the electron velocity distribution. Thus, the phase space volume of particles actively contributing to radiation remains small only, while the phase space volume of absorbing particles increases. Both effects strongly reduce the growth rate to values of 10^{-5}–10^{-7} ω_{ce} such that one expects weak radiation only at higher harmonics. These values imply e-folding times in the range 1–100 s corresponding to e-folding lengths of 3×10^5–3×10^7 km which may be unrealistic.

The remaining possibility for intense radiation is that the radiation source is located very close to the Hermean surface in the strongest magnetic field available and, in addition, that the electron density is depleted by an order of magnitude or more, in which case emission will occur in the electromagnetic X-mode at about $f_{\text{maser}} \sim 8.4$ kHz. Near-planet plasma densities much higher than the one assumed earlier in the range from 10^7 m^{-3}–10^{10} m^{-3} have also been hypothesized (cf. the review by Hunten et al. 1988) in which case the plasma-to-cyclotron frequency ratio is much larger, requiring more violent density depletion factors for the generation of auroral radiation by the known maser mechanisms.

What might dilute the plasma close to Mercury? It is clear that there is no possibility of having low electron densities at low altitude on the illuminated dayside of Mercury. This side is covered by a layer of photoelectrons. However, during the long Mercury night in the shadow of the planet photoelectrons are about absent. Any electrons are either plasma sheet electrons or accompanying ion sputtering. These electrons are magnetically bound. In the

absence of strong plasma diffusion processes (which are not completely excluded, however, because the Hermean magnetic field seems to be highly disturbed and, in addition, presence of high ion densities might contribute to a nonnegligible collisionality) the remaining possibility to deplete them locally on the small scale is by large magnetic-field-aligned potential drops, i.e., by parallel electric fields such as those known from Earth's auroral zone (e.g., Block 1988; Carlson et al. 1998).

Field-aligned potential drops on Earth occur in the presence of field-aligned current flow during substorms, and auroral radio emission correlates with auroral and substorm activity. The question of substorms on Mercury is addressed in a companion paper (Fujimoto et al. 2007).

Substorms are most probably driven by reconnection in the near-planet tail-current sheet. At Mercury the typical substorm time scale is 1–2 min (Baumjohann et al. 2006). Reconnection at Mercury must therefore be fast. This is possible only when the width of the tail current sheet, Δ, is on the order of or less than the ion inertial length $\lambda_i = c/\omega_{pi}$. For the Mariner 10 plasma sheet densities $n_e \sim 3 \times 10^6$ m^{-3}, assuming quasi-neutrality and a pure hydrogen plasma, the shortest ion skin depth is $\lambda_{\mathrm{H}} = 130$ km. For observed heavier ion constituents like Na, K, and O it will be larger by a factor of 2 or 3. The transition time for this length at a convective inflow speed between a few 10 km s^{-1} and a few 100 km s^{-1} is between 10 s and 1 s, barely long enough for letting a fluid or ion instability grow enough to drive a substorm. Reconnection will thus proceed on electron inertial scales $\lambda_e = c/\omega_{pe} \approx 3$ km deep inside the "ion diffusion" Hall current region, which reduces the transition time to between 30 ms and 300 ms. The field-aligned currents are the closure currents of the Hall current system at the reconnection site (Nagai et al. 2001; Oieroset et al. 2001; Treumann et al. 2006). These field-aligned currents are probably carried by low-frequency electromagnetic plasma wave pulses. Since the transverse scale at the reconnection site is the ion inertial length, these waves are kinetic Alfvén waves with dispersion relation

$$\omega_{kA}^2 = k_\parallel^2 v_A^2 \left(1 + k_\perp^2 \rho_i^2\right), \tag{6}$$

where ρ_i is the thermal ion gyroradius. These waves travel along the magnetic field but propagate slowly transverse to the magnetic field thereby deviating from their original field line. Moreover, the waves are large-amplitude nonlinear waves. They also carry a transverse electric field that gives rise to shear motion along the field line where they propagate. In the presence of an ionosphere, current closure and shear motions would imply that the electric potential lines close to the planet deviate from being parallel to the magnetic field. This generates a field-aligned potential drop as large as the transverse electric field shear drop. It is the parallel drop that evaporates the plasma from the field region. By this mechanism a highly diluted plasma would result.

However, in the absence of an ionosphere it is highly uncertain how current closure is achieved and whether such a field-aligned potential drop is actually created. There are two possibilities for current closure in the absence of an ionosphere: either through transverse current diffusion in the thermospheric plasma or through current closure in the planetary body itself. Neither mechanism is understood so far. The former can proceed only via pressure-gradient drift currents which are carried by ions. The latter depends on the conductivity of the Hermean crust and uppermost mantle.

In addition to plasma depletion, in order to radiate, the weakly relativistic electron component must be in an "excited state," i.e., it must carry a substantial amount of free energy with practically no electrons in the lowest (thermal) energy states. Such electron phase space distributions—which in solid state physics are known as "inverted states"—can in a plasma

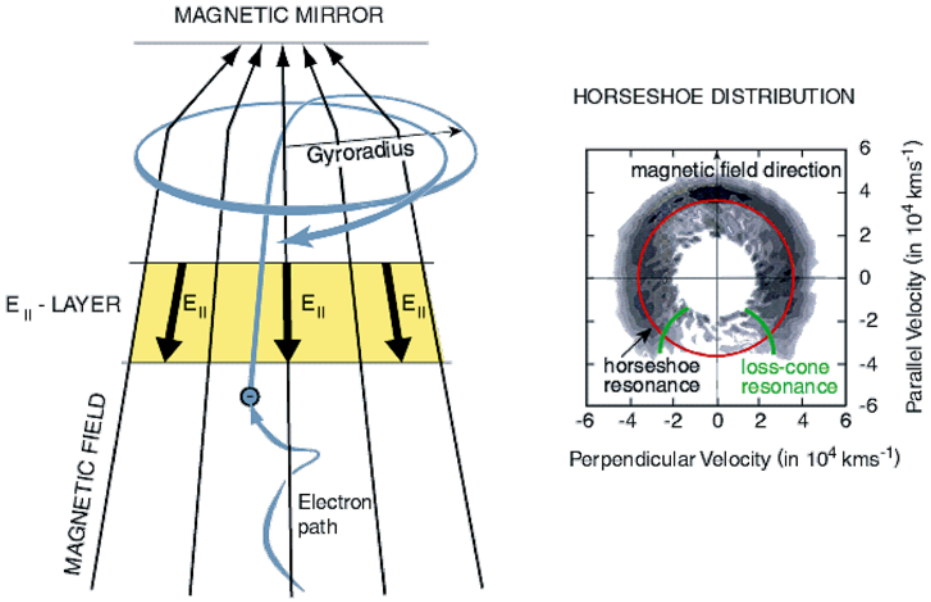

Fig. 5 Evolution of an electron ring-shell phase space distribution in the combined action of a mirror magnetic field and a magnetic field-aligned electrostatic potential drop. *Left*: Schematic of a converging magnetic mirror field geometry. The magnetic mirror is shown highly exaggerated. An electron spiralling along the magnetic field at small gyro-radius picks up the full energy of the electrostatic potential drop when passing the region of a parallel electric field directed away from the mirror point. Behind the electric field layer the parallel electron energy is converted by the magnetic mirror force under conservation of the electron's magnetic moment into perpendicular energy. This happens for all quasi-trapped electrons, i.e., the electrons outside the loss cone. *Right*: The resulting electron distribution in phase space (as has been observed in the terrestrial auroral region by the FAST spacecraft (Delory et al. 1998)) forms a ring that lacks the particles inside the loss cone and practically also lacks all thermal energy electrons. In practice such electrons will still be present due to photo emission from spacecraft. These photoelectrons would occupy the empty inner circle in the figure from where they have been artificially removed (from Treumann 2006)

most easily be generated in the presence of magnetic field-aligned electrostatic potential drops in a mirror magnetic field geometry. The "excited state" in a magnetic mirror without parallel electric field is a loss-cone distribution. This, however, is only weakly excited. Instead, the combined action of a field-aligned electric potential drop and a magnetic mirror produces a strongly excited "ring" or "shell distribution" in phase space by first accelerating the electrons along the field to energies on the order of the potential drop, and then mirroring the accelerated electrons by conserving their magnetic moments.

In this way the electric field energy that is fed into the electrons is transferred to the perpendicular velocity of the electrons, and almost all low-energy electrons are lifted into the excited ring state. This is schematically shown in Fig. 5. One should, however, note that in the weak Hermean magnetic field the mirror force is also weak. Most of the mirror points for the particles lie below the Hermean surface. The equatorial loss cone angle for particles having their mirror point right at the Hermean surface is

$$\sin \alpha_{eq} = R^{-3/2}, \tag{7}$$

where $R = r/R_H$. In the small magnetosphere of Mercury the equatorial loss cone angles are large. For $R = 2$–3 the equatorial loss cone is about 20° wide and near surface occupies

60°. Therefore the loss cone might be much more important at Mercury for the generation of radiation than at Earth, where the loss-cone alone causes only a very small deviation from equilibrium and is thus very ineffective in generating radiation. At Mercury, however, filling almost all the upward half of the phase space the radiative importance of the loss cone is greater. Nevertheless, the conditions for emission in the absence of a magnetic field-aligned electric potential drop are unfavourable since the field-aligned electrons remain at low energy and the frequency ratio $\omega_{pe}/\omega_{ce} > 1$.

To our current knowledge the question whether or not Mercury emits auroral radio radiation is open. Detection, or lack thereof, of such radiation will shed light on the existence of magnetic field-aligned currents and electric potential drops, on the physics of substorms, the existence of reconnection, and on the way field-aligned currents are closed under severe conditions.

4 Bremsstrahlung X-Ray Emissions

Planetary aurorae are accompanied by intense particle precipitation and hence particle impact on the planetary atmosphere. If the atmosphere is sufficiently dense such that the precipitating particles experience frequent collisions with the atmospheric constituents, retardation of the electrons leads to direct emission of bremsstrahlung (braking radiation) X-rays. Figure 6 shows a typical example of PIXIE observations of X-ray emission during the interaction of a CME with Earth's magnetosphere on January 1, 2000, at 1945:00–2000:00 UT. PIXIE was at that time observing the northern hemisphere. The colour coded X-ray emission nicely covers part of the nighttime auroral oval circumventing the northern pole (southern magnetic pole) and consisting of several intense precipitation spots corresponding to the regions of strong substorm and auroral activities.

Observations from 120,000 km distance by the high-resolution X-ray camera (HRC) on Chandra at lower X-ray energies of 0.1–10 keV during aurorae have also been presented recently (Fig. 7a). Similar observations of aurora-related X-ray emissions have been reported for Jupiter. An example is shown in Fig. 7b.

X-rays from Mercury have so far not been observed either due to lack of any X-ray detector on the spacecraft flying by Mercury or to the lack of X-rays originating at Mercury. The Messenger spacecraft, which is currently on its way to Mercury, carries an X-ray spectrometer to measure the composition of the uppermost surface layer of the planet by analyzing solar X-ray photons reflected or scattered from the illuminated side of Mercury, so-called X-ray fluorescence. Seen from far away Mercury acts like a screen for solar X-rays emitted from the corona. Fluorescence measurements have in the past been made from the Moon by Rosat and with higher sensitivity by Chandra. They have also been reported recently from Saturn.

On the nightside of Mercury, any X-ray emission coming from the planet will, however, not be solar-related but should indicate precipitation of particles from the planetary magnetosphere. The Messenger instrument is not an X-ray imager and works at rather high X-ray energies. Since the accelerated electron and ion energies are expected to be lower on Mercury than on Earth it is thus uncertain whether Messenger will be able to detect X-rays from the acceleration process.

5 Bow Shock Radiation

Mercury possesses a solar wind generated bow shock which is a supercritical shock similar to Earth's bow shock though of much smaller extent and thus also smaller radius of cur-

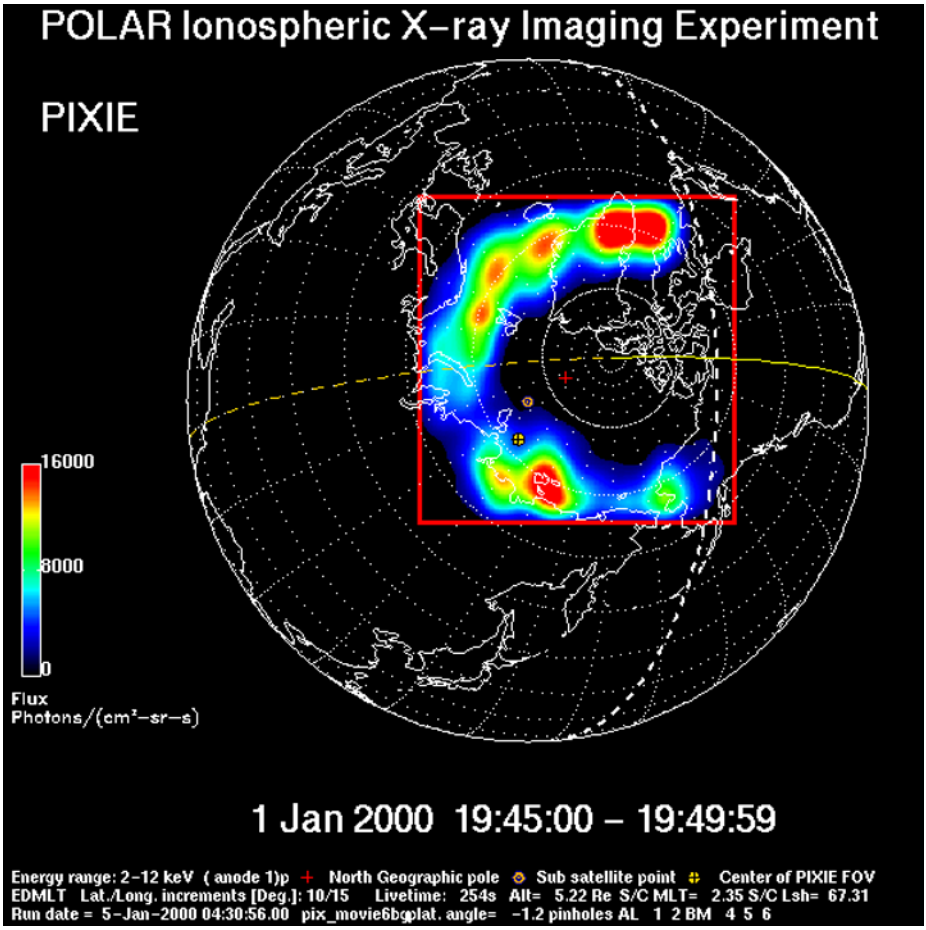

Fig. 6 PIXIE observations of intense auroral X-ray emission during the interaction of a CME with the Earth's magnetosphere (with permission of the PIXIE team, Principal Investigator Dr. Michael Schulz). The observed X-ray emission in the energy range of 2–12 keV nicely maps the nightside part of the auroral oval indicating its direct relation to auroral and substorm activities. The *dashed circle* indicates the position of the terminator at observation time. In addition the emission is spatially highly structured

vature. Because of the small radius of curvature this shock is predominantly parallel and because of the much weaker Hermean magnetic field also dynamically much more active than Earth's and Jupiter's bow shocks. They form and reform continuously, reflect and accelerate solar wind electrons and ions, and possess extended, highly turbulent electron and ion foreshocks. Ultimately, all reflected particles are picked up by the solar wind, i.e., they sense the solar wind electric field in their proper frame of reference and become accelerated up to a few times the solar wind streaming energy. For the electrons this is only a small fraction of their initial thermal energy. However, ions are effectively heated and isotropized by this process.

The mechanism of electron reflection from a supercritical shock is still under investigation. The simplest theories based on the specular reflection assumption refer to the strictly perpendicular region on the bent bow shock surface. At Mercury this region should be ex-

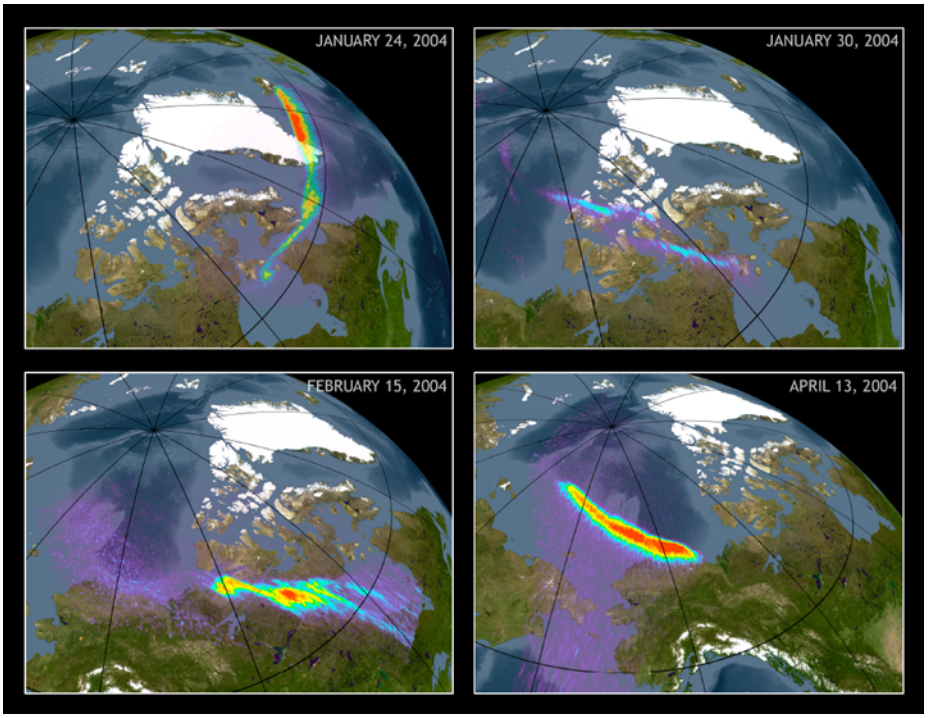

(a)

(b)

Fig. 7 Chandra HRC observations of low energy (0.1–10 keV) auroral X-ray emissions. (**a**) Earth's auroral X-rays detected from 120,000 km distance during early 2004 (courtesy NASA/MSFC/CXC/A.Bhardwaj & R. Elsner et al., *J. Atmos. Terrestr. Phys*., in press). (**b**) A 45-minute Jovian auroral X-ray pulse (*magenta*) on December 18, 2000 (courtesy NASA/SWRI/R. Gladstone et al.), superimposed on the Hubble UV image (*blue*) of Jupiter's aurora. Surprisingly, the position of the pulse does not coincide with the Jovian auroral oval but is shifted closer to the pole, a fact that has not yet been understood properly

tremely narrow, forming a tiny speck only on the shock that is located where the instantaneous interplanetary magnetic field is tangential to the shock surface. Therefore, naively one does not expect large reflected electron fluxes in the foreshock region. This conclusion might, however, be completely wrong and will have to be corrected by observations and refinement of shock electron reflection/acceleration theory when taking into account the shock modification introduced by the reflected ion component.

Supercritical shocks reflect the flow in order to compensate for the excess energy of the inflowing plasma that cannot be transformed into heat and entropy during one shock crossing time. Since reflected electrons carry only a small fraction of the energy of the flow, curved shocks predominantly reflect ions back upstream into the inflowing plasma. Like the electrons these ions form fast beams counter-streaming to the supersonic/superAlfvénic plasma inflow. Since the velocity difference between the ion beams and the flow is far above the ion-acoustic speed, a variety of ion–ion and ion–electron beam instabilities are excited in the foreshock (e.g., Gary 1993). These waves are both electrostatic and electromagnetic.

In Earth's foreshock a number of wave modes excited in this way have been identified. The most interesting ones are the electromagnetic wave modes which propagate in the Alfvénic and magnetosonic ion-whistler branches at low frequency. The spectrum of turbulence to which these waves contribute has also been identified. This spectrum is intermittent since the waves evolve into large amplitude waves which themselves steepen and break. Breaking occurs because of the absence of dissipation and only partial cascading of the waves during the time of flow from their excitation site to the shock proper. But the steepened and breaking waves represent a whole system of small shocklets propagating in the foreshock. These shocklets have at least two effects. First, the turbulence to which they contribute retards the inflow in two ways by extracting flow energy and feeding it into the turbulence, and by trapping and scattering the ions on the ion-gyroscale. Both can be interpreted as collisionless dissipation, and hence the foreshock itself constitutes part of the shock transition. It represents the broadened shock transition region. Second, at the same time the turbulent wave spectrum is convected down to the shock ramp. Since it consists mainly of transverse waves in the Alfvénic and magnetosonic modes it leads to a turnover of the magnetic field direction at the shock front from parallel to perpendicular to the shock normal (in a statistical sense) such that on the ion scale the parallel shock remains quasi-parallel, while on the shorter electron scale the shock is practically quasi-perpendicular. The consequence is that the shock, almost over its entire surface, becomes quasi-perpendicular for electrons and thus is an electron reflector almost everywhere. In this way the electron and ion foreshock are mixed. For Mercury one expects that there is no distinction between electron and ion foreshocks because of the narrowness of the speck where the shock is genuinely perpendicular.

The electron foreshock is populated by electron beams escaping upstream along the solar wind magnetic field. Their effect is to generate Langmuir waves, ion acoustic waves, electron acoustic waves, Buneman modes, and possibly also electromagnetic electron oscillations in the whistler band. All these waves are of substantial interest in structuring the Mercury electron foreshock by formation of Langmuir solitons which may collapse whenever they become more than one-dimensional, ion-acoustic solitons which cause plasma density ripples, electron-acoustic solitons and electron holes, the latter being the consequence of the Buneman instability which also heats the electron plasma. The consequence is a coarse graining of the density in the electron foreshock on the scale of several Debye lengths.

Electron plasma waves have another interesting consequence that may serve as an identifier for electron reflection and particle acceleration. This is the generation of radio wave

emission from the electron foreshock. The basic mechanism is very simple here: Electrostatic waves can be considered as particles. Hence, a three-wave process between waves must conserve energy and momentum. This can be symbolized as

$$L_1 + L_2 + L_3(\text{or } T) = 0,$$

where L denotes longitudinal and T transverse (or electromagnetic). This equation describes either decay of a strong L-wave into other waves or the merging of two L-waves into another wave. In this way higher L-harmonics can be generated by merging, or an electromagnetic high-frequency wave is produced. Both cases are of interest in the electron foreshock. The most common one is the merging of two Langmuir waves into an electromagnetic wave which is described by the process

$$\omega_1 + \omega_2 = \omega, \qquad k_1 + k_2 = k. \tag{8}$$

The unindexed quantities belong to the radiation wave. Clearly, since this is long wavelength, $k \ll k_1, k_2$, and therefore the waves perform a head-on collision with $k_2 \approx k_1$ in order to merge into radiation. At the same time their energies add up, and the radiation is at frequency $\omega \approx 2\omega_1$, say, for Langmuir waves of similar frequencies. Such radiation is at the harmonic of the plasma frequency, $\omega \approx 2\omega_{pe}$, is not absorbed, and can escape from the plasma. This radiation is observed in Earth's foreshock and is expected for Mercury as well if only the Hermean bow shock is strong enough to reflect electrons. In turn, its properties can be used for probing the structure and strength of the bow shock. We should note that similar radiation is generated with other waves, described by similar conservation laws as those above. For instance, the merging of a Langmuir and an ion-acoustic wave produces radiation at the plasma frequency $\omega \approx \omega_{pe}$ since the ion acoustic frequency is much lower than the plasma frequency, and the merging of either a Langmuir wave with an electron acoustic wave produces radiation somewhere above the plasma frequency, $\omega_{pe} < \omega < 2\omega_{pe}$, while merging of two electron-acoustic waves generates just radiation at ω_{pe}. Moreover, bursts of radiation are generated when Langmuir solitons collapse, with highest radiation emission just before the collapse is completed, i.e., at the end of the collapse (Treumann and LaBelle 1992). In this process electrons become accelerated and hot plasma spots are generated in the course of the collapse.

6 Synchrotron Radiation

The elementary form of radiation in (sufficiently strong) magnetic fields is gyro-synchrotron radiation. In contrast to the electron cyclotron maser radiation this type of radiation is incoherent and therefore weak. Gyro-radiation consists of a sequence of emission lines at the electron cyclotron harmonics $\omega = l\omega_{ce}$, $l = 1, 2, \ldots$. These lines are of narrow width. The emissivity decreases with harmonic number. In addition, in hot plasma self-absorption damps the fundamental such that the "second harmonic," $l = 1$, is usually stronger than the fundamental. Gyro-synchrotron radiation depends on the availability of energetic electrons. The emission lines have a narrow but finite spectral width which from the uncertainty relation is proportional to the electron energy/temperature. The higher the temperature/energy the broader are the emission lines, and for relativistic electrons the lines overlap forming a continuous spectrum that decays towards higher frequency. For a power law electron distribution in energy $f(\varepsilon) = A\varepsilon^{-p}$ the total emitted power $P(\omega)$ per unit volume per unit

frequency is

$$P(\omega) = C\frac{e^3 B \sin\alpha}{m_e c^2 (p+1)}\left(\frac{\omega}{\omega_c}\right)^{-(p-1)/2}, \tag{9}$$

where C is a normalization factor that depends on A and p, B is the magnetic field strength, α is the pitch-angle (which can be put to 90°since perpendicular electrons are contributing most; otherwise for a more complicated pitch angle distribution one must average over pitch angle which contributes a numerical factor of order unity), $\omega_c = (3\gamma_{rel}^2\, eB\sin\alpha)/2m_e$ is the critical frequency, and γ_{rel} the relativistic factor which is close to 1 for the expected electron energies in the Hermean magnetosphere. The critical frequency is roughly $\omega_c \approx 1.5\omega_{ce}$. The spectral maximum is then close to $\omega \approx 0.3\omega_c$. The stronger the field and the flatter the electron distribution the higher is the emitted power. We do, however, not expect high emissivities in the magnetosphere of Mercury since the magnetic field is very weak, and the expected electron energies are small such that the electron spectrum will decay steeply with energy. Even synchrotron radiation from Earth's radiation belts is weak, and substantial gyro-synchrotron emissivities in the solar system are measured only from the Sun and Jupiter's magnetosphere.

7 Conclusions and Predictions

ULF waves are known to exist in the Hermean magnetosphere. In addition to being an interesting physical phenomenon in themselves, they can also be used as a diagnostic tool. Their frequency may provide information on the plasma composition, and the phase difference between the electric and magnetic fields of the wave provides information on the reflection coefficient at low altitude, which in turn may be used to estimate the conductivity of the planetary surface or low-altitude (exo)ionosphere.

We are rather pessimistic about the likelihood of radiation from the polar regions of Mercury, a radiation analogue to Earth's AKR and Jupiter's S-bursts. If emitted, the radiation would be around or rather slightly above the local electron cyclotron frequency ($\geq$8 kHz at ground level). This radiation should also be oblique because the condition that the plasma frequency is far below the local cyclotron frequency for fundamental emission is presumably not satisfied. Radiation above the local cyclotron frequency will be very weak, however, because the growth rates are small. On the other hand, intense emission at the fundamental depends on the presence of field-aligned electric potentials close to the planet. Such potentials may evacuate the plasma until $\omega_{pe} < \omega_{ce}$. Whether field-aligned potential drops occur on Mercury is a question of whether reconnection-driven substorms occur in the Hermean magnetosphere. Hence the possible detection of intense auroral radiation with wavelengths of some 100 km at a frequency below or very close to the local cyclotron frequency, transverse propagation in the X-mode and total power of the order of a few percent of the solar wind power transferred to the Hermean magnetosphere would illuminate a number of questions. First, it would suggest that substorms on Mercury exist and are reconnection-related. Second, it would prove that field-aligned electron currents flow from the magnetospheric tail region toward the planet. Third, it would indicate the existence of field-aligned electric potential drops generated in the Hermean magnetosphere, accelerating electrons and making possible electron-maser emission. On the other hand, when weak radiation of much lower power is detected at oblique angles, then it could still be generated by loss-cone distributions. These, however, would be the result from electrons hitting the body of the planet and not from atmospheric loss-cones since the expected atmospheric densities are too low

to efficiently absorb electron fluxes. This is interesting in itself since it would confirm the presence of trapped particle fluxes in the Hermean magnetosphere and associated particle acceleration.

The other radiation source is the bow shock. Similar to Earth's and Jupiter's bow shocks, one expects that the Hermean shock is a strong shock which reflects electrons and ions. Radiation is then generated in the foreshock which for Mercury should fill almost all space upstream of the shock up to the distance that the reflected electron and ion beams can propagate until having dissipated their kinetic energy into feeding wave generation thereby preretarding the solar wind. Some of these waves, in particular Langmuir waves generated by electron beams, are capable of producing radiation at the solar wind plasma frequency $\omega = \omega_{pe}$ and at its second harmonic $\omega = 2\omega_{pe}$. However, other wave modes like electron acoustic and ion-sound waves may be involved as well. From their detection the state of the shock may be inferred.

Acknowledgements Support from the International Space Science Institute, Bern, Switzerland is gratefully acknowledged. Work at the Royal Institute of Technology was supported by the Swedish National Space Board and by the Alfvén Laboratory Centre for Space and Fusion Plasma Physics. The work by KHG was financially supported by the German Ministerium für Wirtschaft und Technologie and the German Zentrum für Luft- und Raumfahrt under contract 50 QW 0602.

References

W. Baumjohann, A. Matsuoka, K.-H. Glassmeier, C.T. Russell, T. Nagai, M. Hoshino, T. Nakagawa, A. Balogh, J.A. Slavin, R. Nakamura, W. Magnes, Adv. Space Res. **68** (2006). doi:10.1016/j.asr.2005.05.117

L.P. Block, Astrophys. Space Sci. **144**, 135 (1988)

L.G. Blomberg, J.A. Cumnock, Y. Kasaba, H. Matsumoto, H. Kojima, Y. Omura, M. Moncuquet, J.-E. Wahlund, Adv. Space Res. **38**, 627–631 (2006)

C.W. Carlson, R.F. Pfaff, J.G. Watzin, Geophys. Res. Lett. **25**, 2013–1016 (1998)

L. Chen, A. Hasegawa, J. Geophys. Res. **79**, 1024–1032 (1974)

G.T. Delory, R.E. Ergun, C.W. Carlson, L. Muschietti, C.C. Chaston, W. Peria, J.P. McFadden, R. Strangeway, Geophys. Res. Lett. **25** (1998). doi:10.1029/98GL00705

M. Fujimoto, W. Baumjohann, K. Kabin, R. Nakamura, J.A. Slavin, N. Terada, L. Zelenyi, Space Sci. Rev. (2007, this issue). doi:10.1007/s11214-007-9245-8

S.P. Gary, in *Theory of Space Plasma Microinstabilities* (Cambridge University Press, 1993), p. 193

K.-H. Glassmeier, P. Mager, D.Y. Klimushkin, Geophys. Res. Lett. **30** (2003). doi:10.1029/2003GL017175

K.-H. Glassmeier, D. Klimushkin, C. Othmer, P. Mager, Adv. Space Res. **33**, 1875–1883 (2004)

D.M. Hunten, T.H. Morgan, D.E. Shemansky, in *Mercury*, ed. by F. Vilas, C.R. Chapman, M.S. Matthews (Univ. Arizona Press, Tucson, 1988), pp. 562–312

H. Matsumoto, J.-L. Bougeret, L.G. Blomberg, H. Kojima, S. Yagitani, Y. Omura, M. Moncuquet, G. Chanteur, Y. Kasaba, J.-G. Trotignon, Y. Kasahara, BepiColombo MMO PWI Team, Adv. Geosci. **3**, 71–84 (2006)

T. Mukai, K. Ogasawara, Y. Saito, Adv. Space Res. (2004). doi:10.1016/S0273-1177(03)00443-5

T. Nagai, I. Shinohara, M. Fujimoto, M. Hoshino, Y. Saito et al., J. Geophys. Res. **106**, 25929–25950 (2001)

N.F. Ness, K.W. Behannon, R.P. Lepping, Y.C. Wang, Nature **255**, 204–205 (1975)

K.W. Ogilvie, J.D. Scudder, V.M. Vasyliunas, R.E. Hartle, G.L. Siscoe, J. Geophys. Res. **82**, 1807–1824 (1977)

C. Othmer, K.-H. Glassmeier, R. Cramm, J. Geophys. Res. **104**, 10,369–10,378 (1999)

M. Øieroset, T.D. Phan, M. Fujimoto, R.P. Lin, R.P. Lepping, Nature **412**, 414–417 (2001)

C.T. Russell, Geophys. Res. Lett. **16**, 1253–1256 (1989)

C.T. Russell, D.N. Baker, J.A. Slavin, in *Mercury*, ed. by F. Vilas, C.R. Chapman, M.S. Matthews (Univ. Arizona Press, Tucson, 1988), pp. 514–561

D.J. Southwood, Planet. Space Sci. **22**, 483–491 (1974)

T. Tamao, Science reports of Tohoku University, Series 5. Geophysics **43**, 43–72 (1965)
R.A. Treumann, Astron. Astrophys. Rev. **13**, 229–315 (2006)
R.A. Treumann, J. LaBelle, Astrophys. J. **399**, L167 (1992)
R.A. Treumann, C.H. Jaroschek, R. Nakamura, A. Runov, M. Scholer, Adv. Space Res. **67** (2006). doi:10.1016/j.asr.2004.11.045
P. Zarka, J. Geophys. Res. **103**, 20,159–20,194 (1998)